

## Light-emitting mechanism varying in Si-rich-SiN<sub>x</sub> controlled by film's composition

Tetyana V. Torchynska <sup>\*1</sup>, Leonardo G. Vega-Macotela <sup>2a</sup>,  
Larysa Khomenkova <sup>3b</sup> and Abdelilah Slaoui <sup>4c</sup>

<sup>1</sup> Instituto Politécnico Nacional, ESFM, Av. IPN, México DF, 07320, México

<sup>2</sup> Instituto Politécnico Nacional, ESIME, Av. IPN, México DF, 07320, México

<sup>3</sup> V. Lashkaryov Institute of Semiconductor Physics at NASU, Av. Nauky 45, Kyiv, 03028, Ukraine

<sup>4</sup> ICube, 23 rue du Loess, BP 20 CR, 67037 Strasbourg Cedex 2, France

(Received October 22, 2016, Revised February 16, 2017, Accepted May 15, 2017)

**Abstract.** Spectroscopic investigation of Si quantum dots (Si-QDs) embedded in silicon nitride was performed over a broad stoichiometry range to optimize light emission. Plasma-enhanced chemical vapor deposition was used to grow the SiN<sub>x</sub> films on Si (001) substrates. The film composition was controlled via the flow ratio of silane (SiH<sub>4</sub>) and ammonia (NH<sub>3</sub>) in the range of  $R = 0.45-1.0$  allowed to vary the Si excess in the range of 21-62 at.%. The films were submitted to annealing at 1100°C for 30 min in nitrogen to form the Si-QDs. The properties of as-deposited and annealed films were investigated using spectroscopic ellipsometry, Fourier transform infrared spectroscopy, Raman scattering and photoluminescence (PL) methods. Si-QDs were detected in SiN<sub>x</sub> films demonstrating the increase of sizes with Si excess. The residual amorphous Si clusters were found to be present in the films grown with Si excess higher than 50 at.%. Multi-component PL spectra at 300 K in the range of 1.5-3.5 eV were detected and non-monotonous varying total PL peak versus Si excess was revealed. To identify the different PL components, the temperature dependence of PL spectra was investigated in the range of 20-300 K. The analysis allowed concluding that the “blue-orange” emission is due to the radiative defects in a SiN<sub>x</sub> matrix, whereas the “red” and “infrared” PL bands are caused by the exciton recombination in crystalline Si-QDs and amorphous Si clusters. The nature of radiative and no radiative defects in SiN<sub>x</sub> films is discussed. The ways to control the dominant PL emission mechanisms are proposed.

**Keywords:** silicon nanocrystals; silicon nitride; photoluminescence; spectroscopic ellipsometry; FTIR

### 1. Introduction

Silicon micro-photonics is getting the significant attention in the field of design and development of Si-based photonic devices offered efficient data transfer with minimum loss as compared to conventional optoelectronics devices. Silicon quantum dots (Si-QDs), either free-standing or embedded in different matrixes (SiO<sub>2</sub>, Si<sub>3</sub>N<sub>4</sub>, Al<sub>2</sub>O<sub>3</sub>, HfO<sub>2</sub>, etc.) have attracted the

\*Corresponding author, Professor, Ph.D., E-mail: [ttorch@esfm.ipn.mx](mailto:ttorch@esfm.ipn.mx)

<sup>a</sup> Ph.D., E-mail: [leo\\_el7sello@hotmail.com](mailto:leo_el7sello@hotmail.com)

<sup>b</sup> Ph.D., E-mail: [khomen@ukr.net](mailto:khomen@ukr.net)

<sup>c</sup> Professor, E-mail: [abdelilah.slaoui@unistra.fr](mailto:abdelilah.slaoui@unistra.fr)

considerable attention over the last decades. Their multifunctional applications in the field of optoelectronics, photonics, photovoltaics, nonvolatile memory, biology, etc. were demonstrated by Chen (Chen *et al.* 2004), Kim (Kim *et al.* 2004), Priolo (Priolo *et al.* 2001), Fauchet (Fauchet *et al.* 2005) and Walters (Walters *et al.* 2005).

It should be noted that most efforts of research laboratories were concentrated on the development of light emitting Si-QDs embedded in a SiO<sub>2</sub> host (Pavesi and Lockwood 2004). However, a large bandgap as well as insulating nature of SiO<sub>2</sub> remain a barrier for the production of electrically pumped light-emitting diodes and efficient photovoltaic cells based on Si-QDs. Additionally, Si-QDs terminated by oxygen atoms demonstrate charge trapping behavior due to the formation of Si = O bonds at the Si-QD/SiO<sub>2</sub> interface. This effect was considered by Wolkin (Wolkin *et al.* 1999) as the main factor of peak independence of the photoluminescence (PL) from oxidized Si-QDs of different sizes. In this regard, oxygen-free materials are considered as most perspective hosts for Si-QDs.

One of them is silicon nitride. It is known that Si<sub>3</sub>N<sub>4</sub> has structural stability upon microelectronic fabrication processing (Belyi *et al.* 1988). Better electrical properties, resulting from its smaller band gap (5.6 eV) than in SiO<sub>2</sub> and lower tunneling barriers, allow the efficient transport of electrons and holes into Si QDs embedded in silicon nitride. The last fact making these films preferable suited for electroluminescent and photovoltaic device applications (Jiang and Green 2006 and Sung *et al.* 2006). Moreover, the photoelectric conversion efficiency can be raised owing to the additional light absorption in Si-QDs and the optical properties of a matrix will be tunable with varying the Si-QD size (Conibeer *et al.* 2006). It is essential that Si-QDs terminated by nitrogen atoms at the Si-QD/Si<sub>3</sub>N<sub>4</sub> interface do not show the limitation in Si-QD emitting energy as demonstrated by Park (Park *et al.* 2001a) and Dal Negro (Dal Negro *et al.* 2005). In addition, Comedi (Comedi *et al.* 2006) and Nalini (Nalini *et al.* 2012) have revealed that the Si-QDs in Si<sub>3</sub>N<sub>4</sub> demonstrate brighter emission than Si-QDs in SiO<sub>2</sub>.

It was shown by Nalini (Nalini *et al.* 2012) as well that the formation of Si-QDs in silicon nitride host requires lower annealing temperature than that in silicon oxide. However, the nucleation and crystallization of Si-QDs in silicon nitride was found to be strongly dependable on the deposition and post-processing conditions (Delachat *et al.* 2009 and Keita *et al.* 2010). Efficient visible emission from Si-rich-Si<sub>3</sub>N<sub>4</sub> (SiN<sub>x</sub>) films prepared by plasma enhanced chemical vapor deposition (PECVD) was already reported by Kim (Kim *et al.* 2004), Torchynska (Torchynska *et al.* 2015a, b), Kistner (Kistner *et al.* 2011), Zeng (Zeng *et al.* 2014) and Wang (Wang *et al.* 2007). The photoluminescence can be tuned from the ultraviolet to near infrared light by adjusting the flow of gases used. It was shown that monitoring the nitrogen-to-silane ratio allowed changing the mean size of amorphous Si clusters in the range of 1.4-2.4 nm followed by the shift of PL peak position from 2.0 to 2.76 eV (Park *et al.* 2001a). Similar shift of PL peak position from 2.0 to 2.96 eV was achieved by Wang (2003), whereas the more prominent variation of PL maxima from 1.38 eV to 3.02 eV was reported by Kim (Kim *et al.* 2004). It was shown by Zeng (Zeng *et al.* 2014) that PL can be controlled via silane-to-ammonia ratio varying also.

It is worth to point that the variation of PL peak position with Si-QD sizes is a basis to attribute observed PL bands to the exciton recombination in Si-QDs. However, in some cases, the different PL peaks were connected with Si-QDs of the same sizes. This fact indicates that PL bands connected with the recombination of excitons inside of Si-QDs or carriers via silicon nitride defects were not clearly discriminated yet.

In some reports (Kim *et al.* 2004, Kim *et al.* 2005, 2006, Park *et al.* 2001a, Torchynska 2015a, Dal Negro *et al.* 2006, Hao and Shen 2008, Rodriguez *et al.* 2012) PL was ascribed to the quantum

confinement effects in Si-QDs. However other authors (Torchynska 2015b, Wang *et al.* 2007, Dal Negro *et al.* 2006) considered the radiative transitions via defects in silicon nitride matrix or via band-tails (Kato *et al.* 2003, Molinari *et al.* 2007, Anutgan *et al.* 2011) as main reasons. Sometimes, the PL peak shift and multicomponent PL spectrum are assigned to light interference in thick SiN<sub>x</sub> films (Rodriguez-Gómez *et al.* 2013). Regardless on the abundance of experimental data, the nature of PL transitions in Si-rich silicon nitride films is still debatable. It should be noted that in the majority papers cited above, the PL study was carried out at 300 K only. Along with this, the discrete excitation energy was used: either UV or visible light that is not enough for the clear conclusion about the origin of optical transitions in Si-rich silicon nitride films. Thus, a detailed PL study of SiN<sub>x</sub> films with different stoichiometry within wide temperature range accompanied by a revision of proposed models for the PL process is required.

## 2. Experimental details

Si-rich silicon nitride films (so-called as SiN<sub>x</sub>) were grown by PECVD method on the p-type (100) silicon substrates from a mixture of silane (SiH<sub>4</sub>, 99.9999% purity) and ammonia (NH<sub>3</sub>, 99.9999%). To achieve the different stoichiometry, the NH<sub>3</sub> flow was varied from 6.3 to 14 sccm at a constant SiH<sub>4</sub> flow (14 sccm). The ratio of flows was given as  $R = [\text{NH}_3]/[\text{SiH}_4] = 0.45\text{--}1.0$  (Table 1). The working pressure, applied bias, plasma power, deposition time and growth temperature were fixed at 0.5 Torr, 70 V, 500 W, 30 min and 300°C, respectively. A conventional annealing at 1100°C for 30 min in nitrogen flow was applied to produce the crystalline Si-QDs.

The films were investigated using the spectroscopic ellipsometry (SE), Fourier transform infrared spectroscopy (FTIR), Raman scattering and photoluminescence (PL) methods. The chemical composition was controlled by Rutherford Back Scattering (RBS) spectroscopy and Elastic Recoil Detection Analysis (ERDA) early in some studied Si-rich silicon nitride films (Delachat 2010). SE method was used to determine optical parameters of the films. The data were collected by means of Jobin-Yvon ellipsometer (UVISEL) where the incident light was scanned in the range of 1.5–4.5 eV under an incident angle of 66.3°. The fitting of experimental data was performed using HORIBA software DeltaPsi2. The uncertainty in the estimation of the refractive index was  $\Delta n = \pm 0.01$ .

Table 1 Technological and physical parameters of SiN<sub>x</sub> films

Parameters	Sample numbers									
	#1	#2	#3	#4	#5	#6	#7	#8	#9	#10
SiH <sub>4</sub> flow (sccm)	14.0									
NH <sub>3</sub> flow (sccm)	14.0	11.6	10.0	9.5	8.8	8.2	7.8	7.4	7.0	6.3
Ratio $R = [\text{NH}_3]/[\text{SiH}_4]$	1.00	0.83	0.71	0.67	0.63	0.59	0.56	0.53	0.50	0.45
$x$ in as-deposited SiN <sub>x</sub>	0.82	0.61	0.50	0.46	0.42	0.39	0.37	0.34	0.30	0.28
[Si excess] in as-deposited films (at.%)	21	34	42	45	48	51	53	56	60	62
QD size $d_{\text{Si-QD}}$ in annealed films (nm)				4.0	4.1	4.2	5.2	5.5	5.9	6.2

FTIR spectra were recorded in the range of 460-4000  $\text{cm}^{-1}$  using a Nicolet Nexus spectrometer under normal and Brewster angle ( $65^\circ$ ) configurations. Raman scattering spectra were investigated using the Jobin-Yvon LabRAM HR 800UV micro-Raman system at 532-nm excitation light of an Ar ion laser with a design presented in Korsunskaja (Korsunskaja *et al.* 2005) and Torchynska (Torchynska *et al.* 2000a).

PL spectra were excited by a 325-nm (3.82eV) line of a He-Cd laser. The power of laser beam was of 80 mW providing pumping a photon flux of about  $1 \times 10^{16}$   $\text{ph/cm}^2 \cdot \text{s}$ . More details about the PL experiment can be found in Torchynska (2000) or Khomenkova (Khomenkova *et al.* 2009). To investigate the evolution of PL spectra with temperature of measurements in the range of 20-300 K, the films were mounted in a closed-cycle helium cryostat. All other experiments were carried out at 300 K.

### 3. Experimental results

#### 3.1 Optical properties of $\text{SiN}_x$ films

It is known (Keita *et al.* 2010) that the excess Si content affects the refractive index of silicon-rich-silicon nitride films. In present study we used spectroscopic ellipsometry to determine optical parameters of  $\text{SiN}_x$  films versus film stoichiometry. The SE spectra consist in the measured  $\Psi$  and  $\Delta$  ellipsometric angles defined from the fundamental equation of ellipsometry  $r_p/r_s = \tan\Psi \exp i\Delta$ , where  $r_p$  and  $r_s$  are the complex reflection coefficients for parallel and perpendicular polarization of light, respectively. To investigate the properties of as-deposited and annealed films, a four-phase optical model was applied. It consists of a silicon substrate; an amorphous non-stoichiometric  $\text{SiN}_x$  layer; a rough surface layer, composed of a mixture of void space and  $\text{SiN}_x$  layers, and air. More details can be found in (Khomenkova *et al.* 2010, Keita *et al.* 2010). To estimate the volume fraction of Si phase in  $\text{SiN}_x$  films, the Bruggeman effective medium approximation (BEMA) has been used (Bruggeman 1935) with the reference for amorphous silicon (a-Si) and stoichiometric  $\text{Si}_3\text{N}_4$ . In this case, a surface roughness was approximated via a 50%-50% BEMA mixture of  $\text{SiN}_x$  and void space.

To fit SE experimental data, the dispersion law for  $n$  and  $k$  was chosen as described by Khomenkova (2010). It is based on the Forouhi–Bloomer (Forouhi and Bloomer 1986) model elaborated for amorphous semiconductor and insulating materials with using an improved parameterization proposed by Jelisson and Modine (1996). The dispersion formulas for  $n$  and  $k$  were given as follows

$$n(\omega) = n_\infty + \frac{B_i \cdot (\omega - \omega_i) + C}{(\omega - \omega_i)^2 + \Gamma_i^2} \quad \text{and} \quad k(\omega) = \begin{cases} \frac{f_i \cdot (\omega - \omega_g)^2}{(\omega - \omega_i)^2 + \Gamma_i^2}, & \omega > \omega_g \\ 0, & \omega \leq \omega_g \end{cases} \quad (1)$$

where  $n_\infty$  is a refractive index at high frequency,  $f_i$  is an oscillator strength,  $\Gamma_j$  is an amortization factor,  $\omega_i$  and  $\omega_g$  are frequencies of free oscillator,  $B_i = f_i \cdot (\Gamma_i^2 - (\omega_i - \omega_g)^2) / \Gamma_i$ ,  $C = 2 \cdot f_i \cdot \Gamma_i \cdot (\omega_i - \omega_g)$ . Two dependences,  $I_s = I \cdot \sin 2\Psi \cdot \sin \Delta$  and  $I_c = I \cdot \sin 2\Psi \cdot \cos \Delta$ , with  $I_0 = E_0 \cdot (|r_p|^2 + |r_s|^2) / 4$ , and  $E_0$  is the amplitude of electric field of incident light, were fitted taking into account a real structure of samples. The model structure and optical properties of the films were optimized by a least-square refinement approach ( $\chi^2$ ) at fitting the experimental data (Table 1). The thickness of  $\text{SiN}_x$  films was found to be in the range of 200-210 nm with the roughness of 2 nm.

Fig. 1(a) shows the dispersion laws obtained for as-deposited SiN<sub>x</sub> films grown with  $R = 1.0, 0.67, 0.63$  and  $0.45$ . The data for the amorphous a-Si ( $n_{\text{Si}}$ ) and Si<sub>3</sub>N<sub>4</sub> ( $n_{\text{Si}_3\text{N}_4}$ ) phases are also given. The dispersion law of as-deposited films approaches the dispersion law of Si<sub>3</sub>N<sub>4</sub> when  $R \rightarrow 1.0$  and that of a-Si when  $R \rightarrow 0$  (Fig. 1(a)).

The refractive indexes for a-Si and Si<sub>3</sub>N<sub>4</sub> can be found in the range  $n_{\text{Si}} = 3.51 \div 4.08$  and  $n_{\text{Si}_3\text{N}_4} = 1.85 \div 2.03$  for 1.95-eV light energy as reported by Philipp (1973). The  $n$  values extracted at 1.95-eV light demonstrate some trend to decrease from  $n = 3.11$  for  $R = 0.45$  down to  $n = 2.36$  at  $R = 1.0$  (Fig. 1(b)) that is in agreement with the results obtained by Keita (Keita *et al.* 2010). The data for  $R = 1.5 - 2.0$  were reproduced from the paper of Keita (Keita *et al.* 2010) and correspond to Si<sub>3</sub>N<sub>4</sub> films.

Based on the BEMA model one can conclude that the  $n$  increases with  $R$  decreasing is governed by rise of the excess Si content in the films. The stoichiometry of as-deposited films can be determined as  $x = [\text{N}]/[\text{Si}]$  taken into account the extracted values for the  $n$  at a given energy (Table 1) from formula proposed by Mackel (Mackel and Ludemann 2001)

$$x = \frac{N}{\text{Si}} = \frac{4}{3} \cdot \frac{n_{\text{a-Si}} - n}{n + n_{\text{a-Si}} - 2n_{\text{a-Si}_3\text{N}_4}} = \frac{4}{3} \cdot \frac{3.67 - n}{n - 0.23} \quad (2)$$

The final simplification was obtained using  $n_{\text{a-Si}_3\text{N}_4} = 1.95$  and  $n_{\text{a-Si}} = 3.67$  for a-Si (Delachat 2010). It turned out that  $R$  increasing from  $R = 0.45$  to  $1.0$  causes varying the  $x$  in the range of  $x = 0.28 - 0.82$  (Table 1). The excess Si content was estimated as  $[\text{Si}_{\text{excess}}] = ((4 - 3x)/(4 + 4x)) \times 100\%$  and it was found to be  $[\text{Si}_{\text{excess}}] = 21\text{-}62\%$  being higher for lower  $R$  values (Table 1).

It is worth to note that the empirical relations between  $n$  and  $x$  do not consider the presence of hydrogen in the films that can affect the results for the Si excess estimation. We have performed the RBS and ERDA analysis for some samples ( $R = 0.50$  and  $1.0$ ) and found that the hydrogen content in as-deposited films decreases from 21.5 at% ( $R = 0.50$ ) to 19 at% ( $R = 1.0$ ) (Table 2). This result can explain the difference in the stoichiometry determined by both methods by the fact that upon deposition the formation of a-Si:H phase can occur in the films similar to the case described in (Sahu *et al.* 2011).

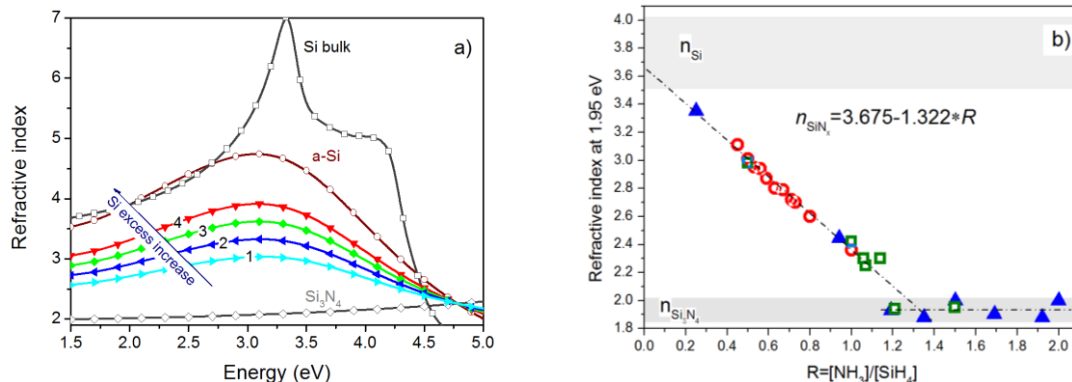


Fig. 1 Dispersion laws (a) for as-deposited SiN<sub>x</sub> films grown at  $R = 1.0$  (1);  $0.67$  (2);  $0.63$  (3) and  $0.45$  (4); Dispersion laws for a-Si, Si<sub>3</sub>N<sub>4</sub> and Si were published early by Delachat (2010) Refractive (b) index (for 1.95-eV light energy) vs  $R$  (circles). Square and triangle symbols from Delachat (2010)

Table 2 Stoichiometry of SiN<sub>x</sub> films

$R = [\text{NH}_3]/[\text{SiH}_4]$	[Si], at%	[N], at%	[H], at%	$x = [\text{N}]/[\text{Si}]$	$n$ at 1.95 eV	$x$ from $n$
0.5	54	24.5	21.5	0.45	3.02	0.37
1.0	45	36.0	19.0	0.80	2.36	0.82

### 3.2 FTIR characterization of the samples

The microstructure of studied films was investigated by FTIR method versus deposition conditions and annealing. The most prominent vibration bands in hydrogenated silicon nitride films grown by PECVD method are usually observed for Si-N ( $470\text{-}490\text{ cm}^{-1}$ ,  $830\text{-}870\text{ cm}^{-1}$ ,  $1190\text{-}1200\text{ cm}^{-1}$ ), Si-H ( $650\text{-}660$  and  $2250\text{-}2300\text{ cm}^{-1}$ ) and N-H ( $1180\text{-}1200$  and  $3340\text{-}3380\text{ cm}^{-1}$ ) vibrations (Tsu 1986, Scardera 2008). Generally, the FTIR spectra of SiN<sub>x</sub> films detected with a normal incidence show significant overlapping of Si-N vibration bands and only one broad band in the range of  $600\text{-}1200\text{ cm}^{-1}$  can be seen (Fig. 3(a)). At the same time, the spectra recorded with a Brewster incidence angle ( $\sim 65^\circ$ ) shows well separated Si-N bands centered at about  $1140$  and  $930\text{ cm}^{-1}$ , ascribed respectively to the longitudinal (LO) and transverse (TO) modes of the Si-N stretching vibration.

FTIR spectra of all studied as-deposited films demonstrate the broad bands with the maxima at  $460\text{-}480\text{ cm}^{-1}$ ,  $830\text{-}880\text{ cm}^{-1}$  and  $1090\text{-}1100\text{ cm}^{-1}$  (Fig. 2(a)). The former band is attributed to the Si-N symmetric stretching vibrations, while two other are caused by transversal and longitudinal modes of asymmetric stretching vibrations, respectively. Their intensities were found to be much higher than those for Si-H and N-H vibrations. The peak position of the Si-N symmetric stretching band depends on the  $R$  value demonstrating the shift to higher wave numbers with  $R$  decreasing (Fig. 2(a)). Such behavior can be explained by increasing the Si content in the plasma, when silicon atoms have not enough nitrogen atoms to form the Si-N bonds. This will cause films' disordering and broadening the FTIR bands (Tsu *et al.* 1986). In contrary, the shift of peak position from  $945.3$  to  $848.6\text{ cm}^{-1}$  is accompanied by band narrowing due to an improvement of SiN<sub>x</sub> film quality (Tomar *et al.* 2008). In our case, the  $R$  decrease results in the higher disorder the SiN<sub>x</sub> films due to increasing the Si excess content. Besides, the lowering of nitrogen content in plasma will stimulate more prominent incorporation of hydrogen in the films. This is evident by the appearance of a shoulder at about  $650\text{-}660\text{ cm}^{-1}$  (Fig. 2(a)) that is also confirmed by the RBS study (Table 2).

High-temperature annealing results in a significant transformation of FTIR spectra (Fig. 2(b)). Si-H related band vanishes due to hydrogen out-diffusion from the films. Simultaneously, the broken Si and N dangling bonds will tend to saturate each other via formation of Si-N and Si-Si bonds, followed by the Si phase appearance. The increase in Si-N peak height at  $1180\text{-}1200\text{ cm}^{-1}$  demonstrates the formation of the Si/SiN<sub>x</sub> interface that is more prominent for films grown at higher  $R$  values (Fig. 2(b)). However, the Si-N peak position at  $900\text{ cm}^{-1}$  points to a significant disordering in the films that can be due to the presence of crystalline Si-QDs and amorphous Si phases (Torchynska *et al.* 2015a). The peak position of Si-N band is well described by a model based on linear combination of weighted bonding density (Tsu *et al.* 1986) that allows determining the film stoichiometry  $x$  (Table 1) using the relation

$$v_{LO} = 323.4 \cdot (x - 0.75) + 1197 \quad (3)$$

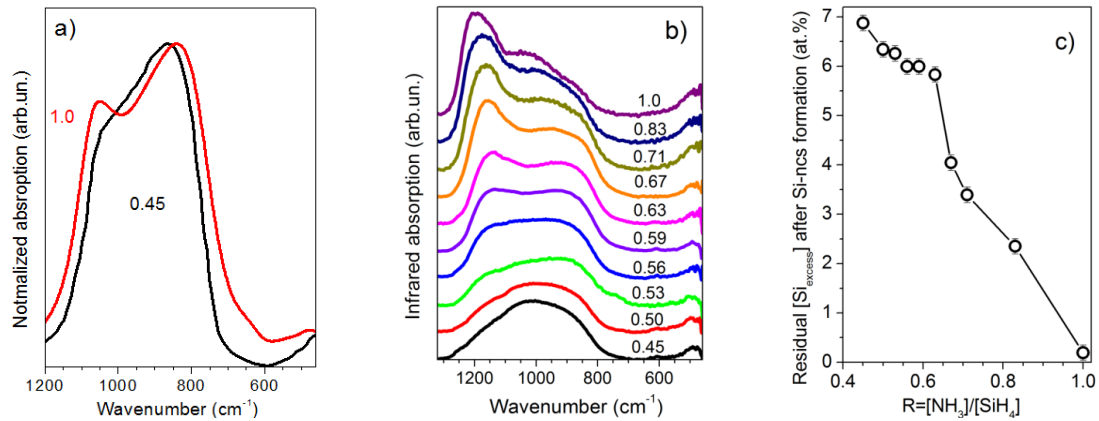


Fig. 2 Brewster-incidence FTIR spectra obtained (a) for as-deposited SiN<sub>x</sub> films with  $R = 0.45$  and  $1.0$ ; and (b) for the films annealed at  $1100^{\circ}\text{C}$  for  $30$  min. The  $R$ -values are shown in the graph. Residual Si excess content (c) in annealed films after the Si-QD formation

This formula is based on the comparison of LO peak variation in studied films with its position in Si<sub>3</sub>N<sub>4</sub> (at about  $1197\text{ cm}^{-1}$ ). Besides, the comparison of LO peak positions in as-deposited and annealed films allows estimating the residual Si excess in annealed films after the Si-QD formation (Fig. 2(c)). In the films grown with  $R > 0.8$  almost all excess Si atoms have been agglomerated into Si-QDs, whereas the films fabricated with lower  $R$  still demonstrate the presence of excess Si (Fig. 2(c)).

### 3.3 Raman scattering study

The Raman scattering study permits to detect the crystalline Si QDs obtained after annealing

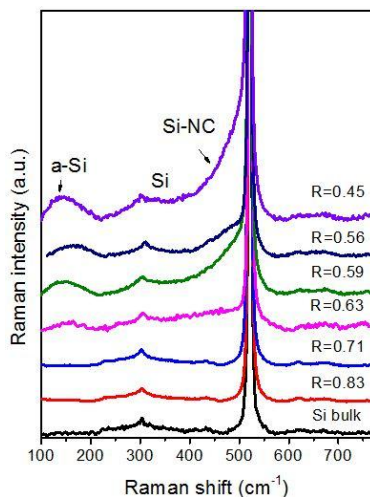


Fig. 3 Raman scattering spectra of SiN<sub>x</sub> films as a function of  $R$  parameters. The spectrum for Si substrate is given for comparison.

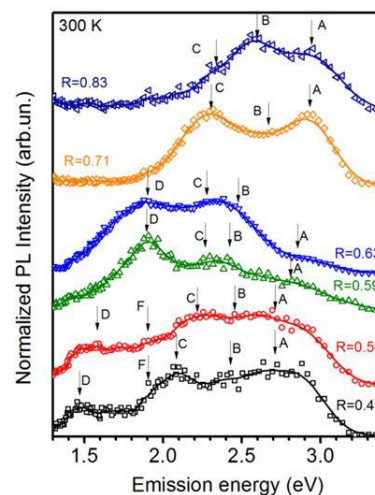


Fig. 4 Evolution of the shape of PL spectra of SiN<sub>x</sub> films with  $R$ . All PL spectra were normalized on their maximal PL intensity.

and to confirm amorphous, a-Si, phase appearing in studied films. The evolution of Raman scattering spectra within the Raman shift range 100-770  $\text{cm}^{-1}$  in the films grown at different  $R$  is presented in Fig. 3 along with the spectrum of the Si substrate.

The diamond structure of Si single crystals allows to detect one first-order Raman active TO-phonon of symmetry  $\Gamma_{25}$  located at the center of Brillouin zone (BZ) with  $\omega_{\text{bulk-Si}} = 520.0 \pm 1.0 \text{ cm}^{-1}$  with the full width at half maximum (FWHM) of 3.5  $\text{cm}^{-1}$  (Johnson and Loudon 1964, Temple and Hathaway 1973). Additionally, the longitudinal acoustic LA(X),  $\omega_{\text{bulk-Si-LA}} = 300 \text{ cm}^{-1}$ , and the longitudinal optical LO(X),  $\omega_{\text{bulk-Si-LO}} = 410 \text{ cm}^{-1}$ , phonons in the X direction were also observed in the Raman spectrum of the Si substrate (Fig. 3). The peak at  $\omega_{2\text{LA}} = 610 \text{ cm}^{-1}$  is overtone of the LA(X) phonon (Johnson and Loudon 1964). Mentioned Raman peaks were detected in Raman scattering spectra of the Si substrate and silicon nitride films grown with  $R = 0.71 - 1.0$  (Fig. 3).

The Raman spectra of annealed films prepared with  $R = 0.45 - 0.67$  present broadening the silicon TO phonon line ( $\omega_{\text{bulk-Si}}$ ) towards 420  $\text{cm}^{-1}$  (Fig. 3). Note that the formation of Si-nanocrystals (NCs) is reflected by the asymmetric shape of TO band and its shift towards lower wavenumbers (Richter *et al.* 1981, Campbell and Fauchet 1986). Thus, the shift of TO ( $\Gamma$ ) phonon to lower frequency (Fig. 3) and its broadening are the evidence of the formation of crystalline Si-QDs.

Additionally, the transverse-acoustic (TA) vibrational mode ( $\omega_{\text{bulk-Si-TA}} = 150 \text{ cm}^{-1}$ ) appears and its intensity increases in the films obtained at  $R = 0.59-0.45$ , which testifies on amorphous Si network appearing even after high-temperature annealing (Torchynska *et al.* 2015a, He *et al.* 2013, Khomenkova *et al.* 2005, Korsunskaya *et al.* 2000). Thus, the signal in the range of 400-530  $\text{cm}^{-1}$  can be considered as overlapping the TO phonons related to the Si substrate, Si-NCs and an amorphous Si phase. Simultaneously, the small bands at 620-630  $\text{cm}^{-1}$  and 730-750  $\text{cm}^{-1}$  in the films with  $R = 0.45-0.67$  are due to silicon nitride, whereas broadening is related to its amorphous or nano-crystalline nature (Torchynska *et al.* 2015b, Muraki *et al.* 1997, Sergo *et al.* 1996, Mercaldo *et al.* 2010, Bandet *et al.* 1999).

### 3.4 Light emitting properties of $\text{SiN}_x$ films

Fig. 4 shows multicomponent PL spectra at 300K obtained for annealed  $\text{SiN}_x$  films with  $R = 0.45-1.0$ . The deconvolution procedure was applied to PL spectra aiming the discrimination of elementary PL bands. The spectral positions and integrated intensities of elementary PL bands depend on the film composition (Fig. 5). The analysis of PL spectra for  $R = 0.71-1.0$  shows three PL bands (Fig. 4) in the “orange-blue” spectral range peaked at 2.90-3.0 eV (A), 2.55-2.75 eV (B) and 2.10-2.25 eV (C).  $R$  parameter decreasing results in the shift of all PL peaks to the lower energy (Figs. 4 and 5(a)). Note that for the samples grown with lower  $R$  the PL bands A, B and C were also detected in PL spectra (Fig. 4). However, for the films grown at  $R = 0.59-0.67$ , the new PL band peaked at 1.90-1.92 eV (D-band) appears and dominates in PL spectra (Figs. 4 and 5(b)). Its peak shifts gradually from 1.90 down to 1.47 eV when  $R$  decreases from  $R = 0.63$  to 0.45 (Figs. 4 and 5(a)). The spectral shift of D-band peak is more significant than the shifts of other PL bands vs  $R$  (Fig. 5(a)). For the films grown with  $R \leq 0.56$  the shoulder at 1.85-1.87 eV (F-band) was determined in PL spectra (Fig. 4).

Fig. 5(b) shows the evolution of integrated PL intensities for the PL bands A, B, C and D versus  $R$ . The PL intensity varies non-monotonously: (i) increases when  $R$  decreases from 1.0 to 0.71; (ii) approaches the highest values for  $R = 0.59-0.67$ ; and (iii) decreases for  $R \leq 0.59$ . Fig. 5(b) represents also varying the optical bandgap of  $\text{SiN}_x$  films vs  $R$  taken from papers of Giorgis

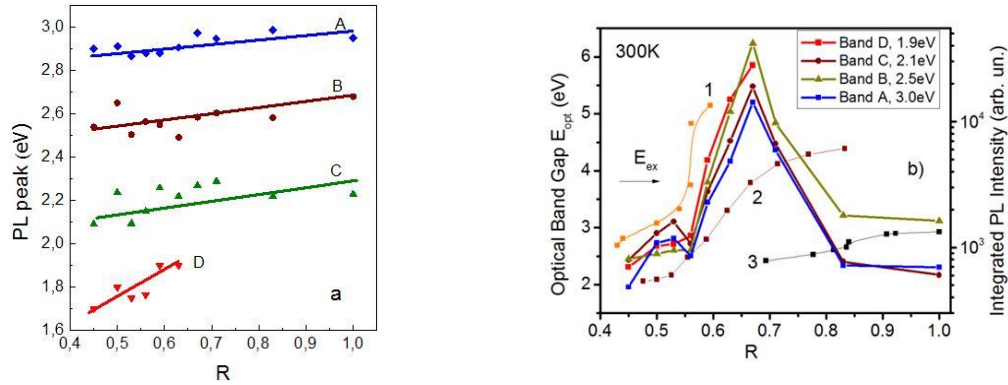


Fig. 5 The variation of PL peak positions (a); and integrated PL intensities (b) for the different PL components with  $R$ . The variation of optical band gap (b); in SiN<sub>x</sub> films vs  $R$  were taken from (1) Giorgis (Giorgis *et al.* 2001); (2) Hsiao (Hsiao *et al.* 2008); and (3) Goncharova (Goncharova *et al.* 2015)

(Giorgis *et al.* 2001), Hsiao (Hsiao *et al.* 2008) and Goncharova (Goncharova *et al.* 2015). It is seen that the results of present work are in the agreement with those from Giorgis (Giorgis *et al.* 2001) and Hsiao (Hsiao *et al.* 2008). This figure shows that the energy of excitation light (3.82eV) becomes equal or exceeds the optical bandgap in films grown at  $R \leq 0.71$  that explains the highest PL intensity observed for films grown at  $R = 0.59-0.67$  (Fig. 5(b)). Simultaneously, the A- and B-bands detected in PL spectra of films grown at  $R = 0.45-0.50$  testifies to their larger optical bandgap (about 3.0 eV) being similar to the data of Giorgis (Giorgis *et al.* 2001).

To gain insight on light-emitting mechanisms in SiN<sub>x</sub> films and to distinguish the types of optical transitions, PL measurements within the range of 20-300 K have been performed (Figs. 6(a)-(d)). The PL bands A, B and C have been detected in whole temperature range for the films with low excess Si content ( $R = 0.71-1.0$ ). Their PL peaks do not change with temperature (Fig. 6(a)) that allows attributing these PL bands to the carrier recombination via native defects in SiN<sub>x</sub> matrix.

The evolution of PL spectra for the film grown at  $R = 0.63$  is shown in Fig. 6(b). The PL peaks of A, B and C bands are unchangeable with temperature as well. However, the D-band peak varies from 1.95-1.97 eV to 1.90-1.92 eV when the temperature increases (Fig. 6(b)). This peak variation (Fig. 7(a)) is similar to the shrinkage of the optical bandgap in the bulk Si crystal and in Si NCs. The change of the Si bandgap vs temperature follows to well-known Varshni equation:

$$E_g(T) = E_g(0) - \frac{\alpha T^2}{\beta + T} \quad (4)$$

where for Si:  $E_g(0) = 1.1692$  eV,  $\alpha = 4.9 \times 10^{-4}$  eV/K and  $\beta = 655$  K (taken from Alex *et al.* 1996). These  $\alpha$  and  $\beta$  parameters are used to fit the temperature variation of the D-band peak (Fig. 7(a)) and the correlation is obtained with the exciton emission varying vs temperature in crystalline Si-QDs.

Figs. 6(c) and (d) show the temperature dependences of PL spectra for the films grown at  $R = 0.56$  and  $0.50$ . Unchangeable PL peaks for A, B and C bands are also detected (Figs. 6(c), (d)). Simultaneously, the peak positions of D- and F-bands vary with temperature (Figs. 6(c), (d) and

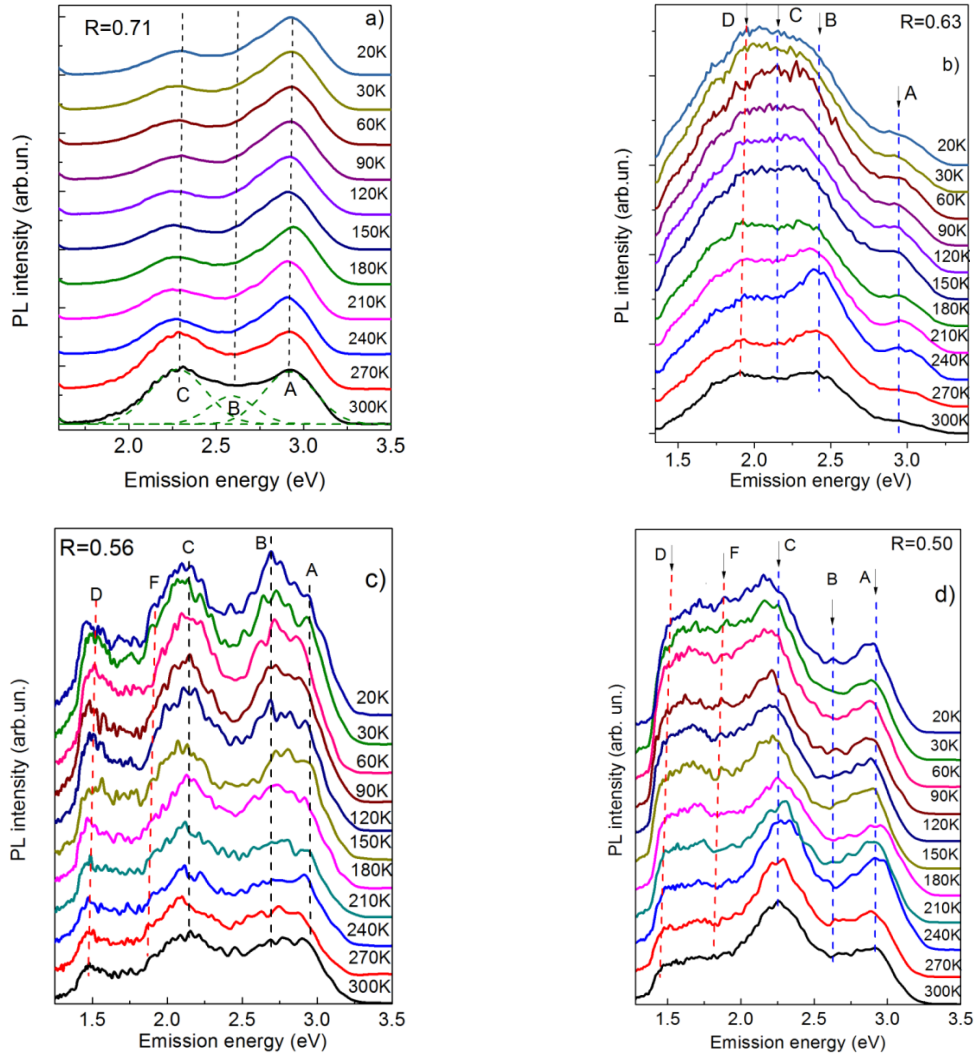


Fig. 6 Evolution of the shape of PL spectra with temperature in the range of 20-300 K for the SiN<sub>x</sub> films grown with  $R = 0.71$ (a);  $0.63$ (b);  $0.56$ (c); and  $0.5$  (d). All spectra were normalized on their maximal PL intensities and shifted in the vertical direction for clarity

7(a)) by the same way as the Si NC bandgap shrinkage that suggests these bands are related to Si phase.

The integrated PL intensities of PL bands A, B, C and D estimated at different temperatures (20-300 K) for the SiN<sub>x</sub> film grown at  $R = 0.63$  are presented in Fig. 7(b). At low temperature ( $\leq 150$  K) the integrated PL intensities of PL bands B, C, D do not change or increases a little for the band A (Fig. 7(b)). The process of PL thermal decay starts for the PL band D at  $T \geq 150$ K and for PL bands A, B and C at  $T \geq 200$ K.

The temperature dependences of integrated PL intensities for all PL bands were fitted on the base of the PL decay model related to the carrier thermal ionization from the defect states to the mobility band edge with some activation energy  $E_a$

$$I(T) = \frac{I_o}{1 - k \exp(-E_a / k_B T)} \quad (5)$$

where  $I_o$  and  $I(T)$  are the integrated PL intensities at low (150 K) and high ( $\geq 150$  K) measured temperatures, and  $k$  is a fitting coefficient. The variation of integrated PL intensities at higher temperatures ( $T \geq 150$  K) has been presented in the Arrhenius plot (Fig. 8). Corresponding activation energies of PL thermal decays are summarized in Table 3.

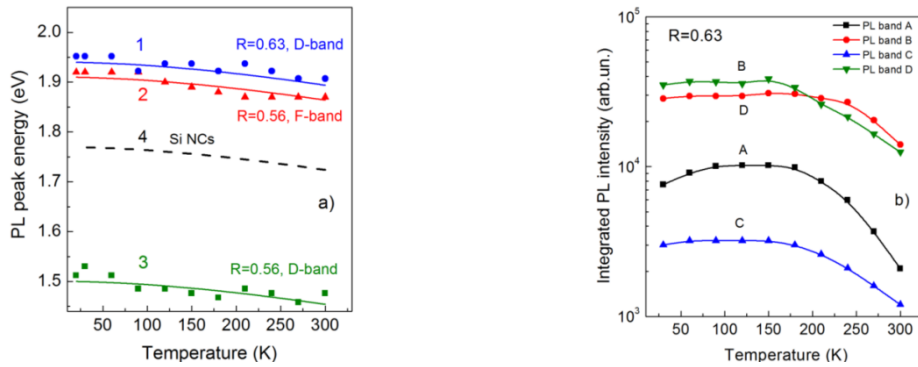


Fig. 7 The variations (a) of the peak positions of PL bands D (1,3) and F(2) with temperature for SiN<sub>x</sub> films grown with  $R = 0.63$  (1) and  $0.56$  (2, 3). Curve 4 represents the shrinkage of the Si NC band gap based on the data taken from Alex (1996). Evolution (b) of integrated PL intensities for the A-D PL bands with temperature for the SiN<sub>x</sub> film grown with  $R = 0.63$

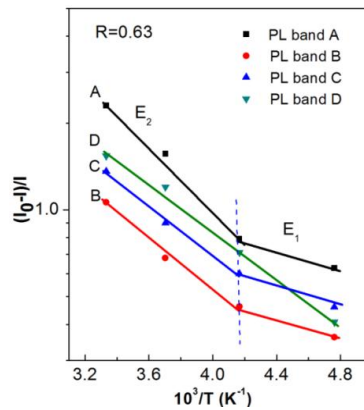


Fig. 8 Arrhenius plot designed for Fig. 7(b)

Table 3 Activation energies of PL thermal decay processes

PL bands	$E_1$ (meV)	$E_2$ (meV)
Band A	32	101
Band B	32	82
Band C	32	79
Band D	71	71

#### 4. Discussion

The analysis of Raman spectra shows that all SiN<sub>x</sub> films can be separated on three sets: (i) grown with  $R = 0.71-1.0$  (set RI); (ii)  $R = 0.67-0.59$  (set RII); and (iii)  $R = 0.59-0.45$  (set RIII). Raman spectra of films from RI-set reveal a low concentration of Si-QDs that is in agreement with negligible broadening the Si TO phonon line in comparison with its FWHM for the Si substrate (Fig. 3). SiN<sub>x</sub> films of a set RII ( $R = 0.59-0.67$ ) demonstrate broadening the Si TO phonon line towards  $420\text{ cm}^{-1}$  (Fig. 3) that testifying on the formation of crystalline Si-QDs. The films from a set RIII ( $R = 0.45-0.59$ ) are characterized by TO phonon broadening as well and by appearing the TA vibrational mode ( $\omega_{\text{Si-TA}} = 150\text{ cm}^{-1}$ ) (Fig. 3). In such films the high concentration of large Si QDs and residual amorphous Si phase are detected (He *et al.* 2013 and Park *et al.* 2001b). The analysis of structural properties allows concluding that high-temperature annealing stimulates the crystallization of Si-QDs in SiN<sub>x</sub> matrix. However, in the films with higher Si content after annealing the residual excess Si (6-7% from FTIR data) can be detected (Fig. 2(c)).

Tuneable room-temperature emission of SiN<sub>x</sub> films has been reported in a set of papers mentioned above, which presented three main explanations for this phenomenon: (i) PL arises from Si-QDs and tuneable emission is related to varying the Si-QD sizes; (ii) PL of SiN<sub>x</sub> films is owing to the radiative transitions between the hydrogen and nitrogen-related chemical bonds located at the Si-QD surface or to the recombination via native defects or dangling bonds in the silicon nitride matrix; (iii) tuneable SiN<sub>x</sub> emission is connected with the recombination via band-tail states. Our experiments show an evolution of PL spectra (Fig. 4) in SiN<sub>x</sub> films grown with fine monitoring the deposition parameters owing to the different PL mechanisms.

Set RI ( $R = 0.71-1.0$ ). The unchangeable peak positions of “orange-blue” PL bands A, B and C with temperature permit to assign these bands to the carrier recombination via defects in SiN<sub>x</sub> matrix. Detected “red” shift of A, B and C PL band peaks vs  $R$  (Fig. 5(a)) is related to the optical bandgap variation with the stoichiometry of SiN<sub>x</sub> films (Fig. 5(b)) (Giorgis *et al.* 2000). A number of studies (Bommali *et al.* 2012, Wang *et al.* 2007, Rui *et al.* 2005, Sain and Das 2013, Deshpande *et al.* 1995, Mo *et al.* 1993, Warren *et al.* 1990) have been devoted to the defect nature investigation in hydrogenated and hydrogen-free silicon nitride matrix. It was detected using the electron spin resonance (ESR) two paramagnetic defects in a SiN<sub>x</sub> matrix: the K center – Si atom with three Si-N bonds and one Si dangling bond (so called K<sup>0</sup>-centers, ~2.40-2.50 eV) and the N center – N atom with two Si-N bonds and one N dangling bond ( $N_4^+ \rightarrow E_v$  and  $E_c \rightarrow N_2^0$ , ~3.0-3.1 eV) (Deshpande *et al.* 1995 and Warren *et al.* 1990). Additionally, the PL band peaked at 590 nm (2.1 eV) was assigned early to oxygen related defects in silicon nitride (Sain and Das 2013). Another interpretation for the “orange” PL band was proposed in (Deshpande 1995), where this band was attributed to the carrier recombination between  $N_4^+$  and  $N_2^0$  energy levels in silicon nitride.

Thus the PL band A (2.85-3.0 eV) can be assigned to the recombination via nitrogen dangling bond levels ( $N_4^+ \rightarrow E_v$  and  $E_c \rightarrow N_2^0$ ). This conclusion is confirmed by decreasing its intensity with Si content rising and N dangling bond decreasing in films grown at  $R \leq 0.71$  (Fig. 4). Intensities of B and C bands increase significantly in PL spectra of films grown with excess Si content ( $R \leq 0.67$ ) that permits to attribute the defects responsible for the PL band B to the K<sup>0</sup>-centers related to Si dangling bonds. The nature of PL band C is not clear yet.

Set RII ( $R = 0.59-0.67$ ). The emission analysis has revealed that the PL band D dominates in PL spectra of these films (Figs. 4 and 6(b)) and demonstrates a shift of PL peaks with heating similar to the shrinkage of the crystalline Si band gap (Fig. 7(a)). The spectral position of band D, the shift

of PL peaks from 1.90 to 1.47 eV with increasing the excess Si content and the correlation of peak D behavior with the shrinkage of the Si NC band gap vs temperature permit to attribute the band D to the exciton recombination in crystalline Si-QDs of different sizes.

The diameter of crystalline Si-QDs can be estimated from the band D peaks using formula  $E = 1.13 + 13.9/d^2$ , which was proposed by Cho (Cho *et al.* 2005) for band-gap increasing with crystalline Si QD size decreasing. Using the value of Stock's shift (~50 meV) for exciton emission in Si-QDs (Torchynska 2010), the crystalline Si-QD sizes are estimated of 4.0-6.2 nm at varying the band D peak from 1.92 to 1.48 eV (Table 1).

The small activation energy (32 meV), detected in these films, which is the same for the A, B and C PL bands (Table 3), is related, apparently, to the activation of some nonradiative recombination centers. The activation energies estimated for thermal decays of the A (101 meV), B (82 meV) and C (79 meV) PL bands are in a good agreement with previously reported data for the carrier thermal ionization from the defect states to the mobility band edge in SiN<sub>x</sub> (Deshpande 1995, Austin *et al.* 1985). The activation energy of PL band D thermal decay (71 meV) can be assigned as well to the carrier thermal ionization from the energy level in crystalline Si-QDs to the mobility band edge in a SiN<sub>x</sub> matrix.

Additionally, one cannot rule out that in a SiN<sub>x</sub> film grown at  $R = 0.63$  the intensities of D and C PL bands increase with cooling faster than that of A and B PL bands (Fig. 6(b)). This effect can be assigned to the close location of the "orange" emitting centers to the crystalline Si-QDs that allows an effective energy exchange between them to be realized. Such a center can be located at the Si-QDs/SiN<sub>x</sub> interface. In the last case, the optical transition between N<sub>4</sub><sup>+</sup> and N<sub>2</sub><sup>0</sup> energy levels proposed early by Deshpande (1995) as a nature of the orange PL band C looks very reliable.

Set RIII ( $R = 0.45-0.59$ ). The integrated PL intensity of all PL bands in the films of this set decreases dramatically with  $R$  (Fig. 5(b)) that can be owing to high residual amorphous Si content and/or crystalline Si-QD size increasing. Actually, the D-band intensity decreases faster, in comparison with others, due to an enlargement of crystalline Si-QD sizes that is accompanied by quenching the exciton emission efficiency inside of QDs (Torchynska 2010). Moreover as far as the quantum confinement effect in Si-QDs is considered, a wider PL spectrum is expected to be for the films with a high Si excess content, since this leads to broadening of the Si-QD size distribution. Actually, our results confirm that PL spectra are broader for the films with high Si excess contents (Figs. 4 and 6(b), (c), (d)).

FTIR and Raman scattering studies confirm that after high temperature annealing the residual excess Si still exists as a-Si phase in SiN<sub>x</sub> films together with embedded crystalline Si-QDs (Fig. 3). The a-Si phase impacts on PL spectra of silicon nitride films via two effects: (i) the nonradiative (NR) recombination rate increases owing to the higher concentration of Si dangling bonds (NR centers in a-Si phase); and/or (ii) the a-Si QD formation that can be responsible for the PL band F (Torchynska 2010).

Actually, integrated PL intensity quenching for all PL bands (Fig. 5(b)) in the films grown at  $R \leq 0.59$  is owing to nonradiative recombination channel appearing, which related obviously to the a-Si phase. Additionally, it is known that the hydrogenated a-Si:H phase due to the passivation of Si dangling bonds by hydrogen can be considered as a mixture of different size a-Si QDs (Torchynska 2010). Moreover, it was shown early using the FTIR method that the hydrogenated SiN<sub>x</sub> films contain hydrogen in the form of Si-H bonds even after 5 hours of annealing at the temperature 1130°C (Bugaev *et al.* 2012). Thus, the a-Si phase in hydrogenated SiN<sub>x</sub> films can be considered, at least partially, as a mixture of a-Si QDs as well.

In PL spectra of SiN<sub>x</sub> films grown with  $R \leq 0.59$  an additional PL band F peaked at 1.85-1.87

eV has been detected (Figs. 4 and 6(c), (d)). The correlation of peak F shift with the shrinkage of the bulk Si band gap versus temperature (Fig. 7(a)) permits to assign this band to the exciton recombination inside of a-Si-QDs. The size of a-Si-QDs can be estimated from the F-band peak positions using the relation  $E = E_{g0} + 2.4/d^2$ , which was proposed early for the band-gap energy increasing at decreasing the a-Si-QD size (Park *et al.* 2001a). Taking  $E_{g0}$  for the a-Si phase equal to 1.79–1.82 eV (Fukutani *et al.* 1998, Abdulraheem *et al.* 2014), the size of a-Si QDs is estimated within the range of 5–7 nm. Thus, the multichannel PL in SiN<sub>x</sub> films grown at highest Si excess ( $R = 0.45\text{--}0.56$ ) includes the carrier recombination via native defects in SiN<sub>x</sub> as well as exciton emission in crystalline Si-QDs and in amorphous a-Si QDs.

The influence of different environments on the emission of Si QDs embedded in silicon nitride has been discussed in a set of papers (Lan *et al.* 2009, Hao *et al.* 2008, Wenge *et al.* 2008). In Si-rich nitride films, which were fabricated by atmospheric pressure chemical vapor deposition (APCVD) in N<sub>2</sub> or H<sub>2</sub> atmospheres (Lan *et al.* 2009), one dominated PL line at 2.5–2.6 eV was revealed in PL spectra. This line was attributed to exciton emission in Si QDs. Additionally, the film fabricated in N<sub>2</sub> presented two high energy peaks at 2.94 and 3.29 eV, while the film deposited in H<sub>2</sub> demonstrated only one satellite peak at 3.40 eV. These different high energy satellite peaks were attributed to the different surface states at the Si QD interface in the SiN<sub>x</sub> films obtained in the different gas ambiances (Lan *et al.* 2009) that correlate with our defect-related interpretation of the high energy PL band 2.9–3.0 eV in studied SiN<sub>x</sub> films.

The photoluminescence at 1.90 eV of Si QDs embedded in hydrogenated amorphous silicon nitride and annealed in oxygen ambient was investigated in Hao *et al.* (2008). It was proposed that the luminescence of the oxidized samples originates from the localized exciton radiative recombination via the surface states related to Si–N or Si–O–Si (Hao *et al.* 2008). Note that the emission of excitons via the Si = O surface state in Si QDs embedded in silicon oxide matrix was investigated in details early (Wolkin *et al.* 1999, Pavesi and Lockwood 2004, Torchynska 2010). It was shown that Si- QDs coordinated with oxygen atoms are subject to charge trapping at the interface, which limits the energy of emission quanta from Si-QDs to less than 2 eV (Wolkin *et al.* 1999). Actually the great interest to Si QDs embedded in silicon nitride just has been motivated by the expectation that Si- QDs coordinated with nitrogen atoms do not exhibit the same emission quanta limitation. Note that the emission peak of Si QDs at 1.90 eV detected in Hao *et al.* (2008) coincides with the PL band D (1.90–1.92 eV) attributed to Si QDs in presented paper.

Finally, the Si-rich SiN<sub>x</sub>: H films prepared by helicon wave plasma-enhanced chemical vapor deposition (HWP-CVD) technique and post-annealed at 800 °C in the (i) H<sub>2</sub>; (ii) FG (10% H<sub>2</sub> in N<sub>2</sub>); and (iii) N<sub>2</sub> ambient were studied in Wenge *et al.* (2008). The main effect detected was connected with the formation of new Si–N bonds owing to the breaking of both Si–H and N–H bonds at annealing due to the effusion of hydrogen. Unfortunately these authors did not study the PL modification in Si-rich-SiN<sub>x</sub> films at annealing mentioned above with different environments. However the authors (Wenge *et al.* 2008) detected that the optical absorption coefficient in the sub-band gap significantly increases after the thermal annealing process. This sub-band gap absorption was attributed to the optical absorption of silicon dangling bonds at Si cluster surface that correlate with our conclusions as well.

## 5. Conclusions

Silicon-rich-silicon nitride films with different stoichiometry were fabricated by PECVD on the Si substrates. It was demonstrated that spectroscopic ellipsometry and FTIR methods allow

estimating the composition of SiN<sub>x</sub> films. The investigation of PL spectra within 20-300 K gives opportunity to extract the information about the contribution of different radiative channels in emission of SiN<sub>x</sub> films with embedded Si-QDs. The unchangeable peak positions of “orange-blue” PL bands A, B and C with temperature permit to assign these bands to the carrier recombination via defects in SiN<sub>x</sub> matrix. At the small level of Si excess content ( $R = 0.71-1.0$ ) the emission via native defects in SiN<sub>x</sub> dominates.

Exciton emission inside of small size (4.0-4.2 nm) crystalline Si-QDs is the main recombination mechanism in the films grown at higher Si excess ( $R = 0.59-0.67$ ), which was confirmed by a shift of PL peak D with heating similar to the shrinkage of the crystalline Si band gap. The multichannel emission is detected in SiN<sub>x</sub> films grown at highest Si excess ( $R = 0.45-0.59$ ): the carrier recombination via native defects in SiN<sub>x</sub> (PL bands A, B and C), exciton emissions in big (5.2-6.2 nm) crystalline Si-QDs (PL band D) and inside of a-Si-QDs with the size of 5-7 nm (PL band F). The optimal conditions for the achievement of the high PL intensity are determined within the R parameter range of 0.59-0.67 for SiN<sub>x</sub> films.

## Acknowledgments

The authors would like to thank SIP-IPN (project 20170821) and CONACYT (project 258224) of Mexico, National Academy of Sciences of Ukraine and Center of National Scientific Research (CNRS) of France for the financial support via program “Dnipro”.

## References

- Abdulraheem, Y., Gordon, I., Bearda, T., Meddeb, H. and Poortmans, J. (2014), “Optical bandgap of ultra-thin amorphous silicon films deposited on crystalline silicon by PECVD”, *AIP Advances*, **4**(5), 057122.
- Alex, V., Finkbeiner, S. and Weber, J., (1996), “Temperature dependence of the indirect energy gap in crystalline silicon”, *J. Appl. Phys.*, **79**(9), 6943-6946.
- Anutgan, M., Anutgan, T., Atilgan, I. and Katircioglu, B. (2011), “Photoluminescence analyses of hydrogenated amorphous silicon nitride thin films”, *J. Lumin.*, **131**(7), 1305-1311.
- Austin, I.G., Jackson, W.A., Searle, T.M., Bhat, P.K. and Gibson, R.A. (1985), “Photoluminescence properties of a-SiN<sub>x</sub>: H alloys”, *Philos. Mag. B*, **52**(3), 271-288.
- Bandet, J., Despax, B. and Caumont, M. (1999), “Nitrogen bonding environments and local order in hydrogenated amorphous silicon nitride films studied by Raman spectroscopy”, *J. Appl. Phys.*, **85**(11), 7899-7904.
- Belyi, V.I., Vasilyeva, L.L., Gennann, R., Ginovker, A.S., Gritsenko, V.A., Repinsky, S.M., Sinitza, S.P., Smirnova, T.P. and Edelman, F.L. (1988), *Silicon Nitride in Electronics, Materials Science*, Monographs, Volume 34, Elsevier Science Ltd., Amsterdam, Netherlands.
- Bommali, R.K., Singh, S.P., Rai, S., Mishra, P., Sekhar, B.R., Prakash, G.V. and Srivastava, P. (2012), “Excitation dependent photoluminescence study of Si-rich a-SiN<sub>x</sub>: H thin films”, *J. Appl. Phys.*, **112**(12), 123518.
- Bruggeman, D.A.G. (1935), “Berechnung verschiedener physikalischer Konstanten von heterogenen Substanzen. I. Dielektrizitätskonstanten und Leitfähigkeiten der Mischkörper aus isotropen Substanzen”, *Ann. Phys.*, **416**, 636-664.
- Bugaev, K.O., Zelenina, A.A. and Volodin, V.A. (2012), “Vibrational spectroscopy of chemical species in silicon and silicon-rich nitride thin films”, *Int. J. Spectroscopy*, **2012**, 281851.
- Campbell, I.H. and Fauchet, P.M. (1986), “The effects of microcrystal size and shape on the one phonon

- Raman spectra of crystalline semiconductors”, *Sol. St. Commun.*, **58**(10), 739-741.
- Chen, M.J., Yen, J.L., Li, J.Y., Chang, J.F., Tsai, S.C. and Tsai, C.S. (2004), “Stimulated emission in a nanostructured silicon pn junction diode using current injection”, *Appl. Phys. Lett.*, **84**(12), 2163-2165.
- Cho, C.H., Kim, B.H., Kim, T.W., Park, S.J., Park, N.M. and Sung, G.Y. (2005), “Effect of hydrogen passivation on charge storage in silicon quantum dots embedded in silicon nitride film”, *Appl. Phys. Lett.*, **86**(14), 143107.
- Comedi, D., Zalloum, O.H.Y, Wojcik, J. and Mascher, P. (2006), “Light emission from hydrogenated and unhydrogenated Si-nanocrystal/Si dioxide composites based on PECVD-grown Si-rich Si oxide films”, *IEEE J. Sel. Top. Quant. Elect.*, **12**(6), 1561-1569.
- Conibeer, G., Green, M., Corkish, R., Cho, Y., Cho, E.C., Cho, C.W., Jiang, C.W., Fangsuwannarak, T., Pink, W., Huang, Y., Puzzer, T., Trupke, T., Richards, B., Shalav, A. and Lin, K.L. (2006), “Silicon nanostructures for third generation photovoltaic solar cells”, *Thin Solid Films*, **511-512**, 654-662.
- Dal Negro, L., Yi, J.H., Nguyen, V., Yi, Y., Michel, J. and Kimerling, L.C. (2005), “Spectrally enhanced light emission from aperiodic photonic structures”, *Appl. Phys. Lett.*, **86**(26), 261905.
- Dal Negro, L., Yi, J.H., Kimerling, L.C., Hamel, S., Williamson, A. and Galli, G. (2006), “Light emission from silicon-rich nitride nanostructures”, *Appl. Phys. Lett.*, **88**(18), 183103.
- Delachat, F. (2010), “Elaboration and characterization of si-licon nanoparticles in silicon nitride for photovoltaic application”, Ph.D. Thesis; InESS-University of Strasbourg, Strasbourg, France.
- Delachat, F., Carrada, M., Ferblantier, G., Grob, J-J. and Slaoui, A. (2009), “Properties of silicon nanoparticles embedded in SiN<sub>x</sub> deposited by microwave-PECVD”, *Nanotechnology*, **20**(41), 415608.
- Deshpande, S.V. and Gulari, E., Brown, S.W. and Rand, S.C. (1995), “Optical properties of silicon nitride films deposited by hot filament chemical vapor deposition”, *J. Appl. Phys.*, **77**, 6534-6541.
- Fauchet, P.M., Ruan, J., Chen, H., Pavesi, L., Dal Negro, L., Cazzanelli, M., Elliman, R.G., Smith, N., Samoc, M. and Luther-Davies, B. (2005), “Optical gain in different silicon nanocrystal systems”, *Opt. Mater.*, **27**(5), 745-749.
- Forouhi, A.R. and Bloomer, I. (1986), “Optical dispersion relations for amorphous semiconductors and amorphous dielectrics”, *Phys. Rev. B*, **34**(10), 7018-7026.
- Giorgis, F., Vinegoni, C. and Pavesi, L. (2000), “Optical absorption and photoluminescence properties of a-Si<sub>1-x</sub>N<sub>x</sub>: H films deposited by plasma-enhanced CVD”, *Phys. Rev. B*, **61**(7), 4693-4698.
- Goncharova, L.V., Nguyen, P.H., Karner, V.L., D’Ortenzio, R., Chaudhary, S., Mokry, C.R. and Simpson, P.J. (2015), “Si quantum dots in silicon nitride: Quantum confinement and defects”, *J. Appl. Phys.*, **118**(22), 224302.
- Fukutani, K., Kanbe, M., Futako, W., Kaplan, B., Kamiya, T., Fortmann, C.M. and Shimizu, I. (1998), “Band gap tuning of a-Si: H from 1.55 eV to 2.10 eV by intentionally promoting structural relaxation”, *J. Non-Crystal. Solid.*, **227-230**, 63-67.
- Hao, H.L. and Shen, W.Z. (2008), “Identification and control of the origin of photoluminescence from silicon quantum dots”, *Nanotechnology*, **19**(45), 455704.
- Hao, H.L., Wu, L.K. and Shen, W.Z. (2008), “Controlling the red luminescence from silicon quantum dots in hydrogenated amorphous silicon nitride films”, *Appl. Phys. Lett.*, **92**(12), 121922.
- He, J., Wang, Ch., Li, W., Qi, K.-Ch. and Jiang, Y.-D. (2013), “Effect of gas temperature on the structural and optoelectronic properties of a-Si:H thin films deposited by PECVD”, *Surf. Coat. Technol.*, **214**, 131-137.
- Hsiao, H.L., Yang, A.B. and Hwang, H.L. (2008), “Luminescence and structural properties of silicon-rich nitride by X-ray absorption spectroscopy”, *J. Phys. Chem. Sol.*, **69**(2), 278-283.
- HORIBA Software (2012), <http://www.horiba.com/scientific/products/ellipsometers/>
- Jelisson Jr., G.E. and Modine, F.A. (1996), “Parameterization of the optical functions of amorphous materials in the interband region”, *Appl. Phys. Lett.*, **69**(3), 371-374.
- Jiang, C.W. and Green, M.A. (2006), “Silicon quantum dot superlattices: Modeling of energy bands, densities of states, and mobilities for silicon tandem solar cell applications”, *J. Appl. Phys.*, **99**(11), 114902.
- Johnson, F.A. and Loudon, R., (1964), “Critical-point analysis of the phonon spectra of diamond, silicon and

- germanium", *Proc. R. Soc. Lond. A*, **281**(1385), 274-290.
- Kato, H., Kashio, N., Ohki, Y., Seol, K.S. and Noma, T. (2003), "Band-tail photoluminescence in hydrogenated amorphous silicon oxynitride and silicon nitride films", *J. Appl. Phys.*, **93**(1), 239-244.
- Keita, A.-S., Naciri, A.E., Delachat, F., Carrada, M., Ferblantier, G. and Slaoui, A. (2010), "Spectroscopic ellipsometry investigation of the optical properties of nanostructured Si/SiN<sub>x</sub> films", *J. Appl. Phys.*, **107**(9), 093516.
- Khomenkova, L., Korsunskaya, N., Sheinkman, M., Stara, T., Torchynska, T.V. and Vivas Hernandez, A. (2005), "Radiative channel competition in silicon nanocrystallites", *J. Lumin.*, **115**(3), 117-121.
- Khomenkova, L., Gourbilleau, F., Cardin, J., Jambois, O., Garrido, B. and Rizk, R. (2009), "Long lifetime and efficient emission from Er<sup>3+</sup> ions coupled to Si nanoclusters in Si-rich SiO<sub>2</sub> layers", *J. Lumin.*, **129**(12), 1519-1523.
- Khomenkova, L., Cardin, J., Portier, X. and Gourbilleau, F. (2010), "Thermal stability of high-k Si-rich HfO<sub>2</sub> layers grown by RF magnetron sputtering", *Nanotechnology*, **21**(28), 285707.
- Kim, T.Y., Park, N.M., Kim, K.H., Sunga, G.Y., Ok, Y.W., Seong, T.Y. and Choi, C.J. (2004), "Quantum confinement effect of silicon nanocrystals in situ grown in silicon nitride films", *Appl. Phys. Lett.*, **85**(22), 5355-5357.
- Kim, B.H., Cho, C.H., Kim, T.W., Park, N.M., Sung, G.Y. and Park, S.J. (2005), "Photoluminescence of silicon quantum dots in silicon nitride grown by NH<sub>3</sub> and SiH<sub>4</sub>", *Appl. Phys. Lett.*, **86**(9), 091908.
- Kim, T.W., Cho, C.H., Kim, B.H. and Park, S.J. (2006), "Quantum confinement effect in crystalline silicon quantum dots in silicon nitride grown using SiH<sub>4</sub> and NH<sub>3</sub>", *Appl. Phys. Lett.*, **88**(12), 123102.
- Kistner, J., Chen, X., Weng, Y., Strunk, H.P., Schubert, M.B. and Werner, J.H. (2011), "Photoluminescence from silicon nitride - no quantum effect", *J. Appl. Phys.*, **110**(2), 023520.
- Korsunskaya, N., Bulakh, B., Jumayev, B., Khomenkova, L., Yukhymchuk, V. and Torchynska, T. (2005), "Raman scattering characterization of macro- and nanoporous silicon", *Appl. Surf. Sci.*, **243**(1), 30-35.
- Korsunskaya, N.E., Torchinskaya, T.V., Khomenkova, L.Yu., Dzhumaev, B.R. and Prokes, S.M., (2000), "Suboxide-related centre as the source of the intense red luminescence of porous Si", *Microelec. Eng.*, **51-52**, 485-493.
- Lan, Sh.M., Huang, Y.Ch., Liao, S.M., Li, Zh.Y., Yang, T.N., Ku, Ch.T., Chen, M.Ch. and Huang, Y.H. (2009), "Luminescence mechanisms of silicon-rich nitride films fabricated by atmospheric pressure chemical vapor deposition in N<sub>2</sub> and H<sub>2</sub> atmospheres", *J. Appl. Phys.*, **105**(5), 053107.
- Mackel, H. and Ludemann, R. (2001), "Detailed study of the composition of hydrogenated SiN<sub>x</sub> layers for high-quality silicon surface passivation", *J. Appl. Phys.*, **92**(5), 2602-2609.
- Mercaldo, L.V., Esposito, E.M., Veneri, P.D., Fameli, G., Mirabella, S. and Nicotra, G. (2010), "First and second-order Raman scattering in Si nanostructures within silicon nitride", *Appl. Phys. Lett.*, **97**(15), 153112.
- Mo, C.M., Zhang, L.D., Xie, C.Y. and Wang, T. (1993), "Luminescence of nanometer-sized amorphous silicon nitride solids", *J. Appl. Phys.*, **73**(10), 5185-5189.
- Molinari, M., Rinnert, H. and Vergnat, M. (2007), "Evolution with the annealing treatments of the photoluminescence mechanisms in a-SiN<sub>x</sub>: H alloys prepared by reactive evaporation", *J. Appl. Phys.*, **101**(12), 123532.
- Muraki, N., Katagiri G., Sergo, V., Pezzotti, G. and Nishida, T. (1997), "Mapping of residual stresses around an indentation in β-Si<sub>3</sub>N<sub>4</sub> using Raman spectroscopy", *J. Mater. Sci.*, **32**(20), 5419-5423.
- Nalini, R.P., Khomenkova, L., Debieu, O., Cardin, J., Dufour, C., Carrada, M. and Gourbilleau, F. (2012), "SiO<sub>x</sub>/SiN<sub>y</sub> multilayers for photovoltaic and photonic applications", *Nanoscale Res. Lett.*, **7**(1), 124.
- Park, N.M., Choi, C.J., Seong, T.Y. and Park, S.J. (2001a), "Quantum confinement in amorphous silicon quantum dots embedded in silicon nitride", *Phys. Rev. Lett.*, **86**(7), 1355-1357.
- Park, N.M., Kim, T.S. and Park, S.J. (2001b), "Band gap engineering of amorphous silicon quantum dots for light-emitting diodes", *Appl. Phys. Lett.*, **78**(17), 2575-2577.
- Pavesi, L. and Lockwood, D.J. (2004), *Silicon Photonics*, Springer-Verlag Berlin, Heidelberg, Germany.
- Philipp, H.R. (1973), "Optical properties of silicon nitride", *J. Electrochem. Soc.*, **120**(2), 295-300.
- Priolo, F., Franzo, G., Pacifici, D., Vinciguerra, V., Iacona, F. and Irrera, A. (2001), "Role of the energy

- transfer in the optical properties of undoped and Er-doped interacting Si nanocrystals”, *J. Appl. Phys.*, **89**(1), 264-272.
- Richter, H., Wang, Z.P. and Ley, L. (1981), “The one phonon Raman spectrum in microcrystalline silicon”, *Sol. St. Commun.*, **39**(5), 625-629.
- Rodriguez, A., Arenas, J. and Alonso, J.C. (2012), “Photoluminescence mechanisms in silicon quantum dots embedded in nanometric chlorinated-silicon nitride, films”, *J. Lumin.*, **132**(9), 2385-2389.
- Rodriguez-Gómez, A., García-Valenzuela, A., Haro-Poniatowski, E. and Alonso-Huitrón, J.C. (2013), “Effect of thickness on the photoluminescence of silicon quantum dots embedded in silicon nitride films”, *J. Appl. Phys.*, **113**(23), 233102.
- Rui, Y., Chen, D., Xu, J., Zhang, Y., Yang, L., Mei, J., Ma, Z., Cen, Z, Li, W., Xu, L., Huang, X. and Chen, K. (2005), “Hydrogen-induced recovery of photoluminescence from annealed a-Si: H/a-SiO<sub>2</sub> multilayers”, *J. Appl. Phys.*, **98**(3), 033532.
- Sahu, B.S., Delachat, F., Slaoui, A., Carrada, M., Ferblantier, G. and Muller, D. (2011) “Effect of annealing treatments on photoluminescence and charge storage mechanism in silicon-rich SiN<sub>x</sub>: H films”, *Nanoscale Res. Lett.*, **6**(1), 178.
- Sain, B. and Das, D. (2013), “Tunable photoluminescence from nc-Si/a-SiN<sub>x</sub>: H quantum dot thin films prepared by ICP-CVD”, *Phys. Chem. Chem. Phys.*, **15**(11), 3881-3888.
- Scardera, G., Puzzer, T., Perez-Wurfl, I. and Conibeer, G. (2008), “The effects of annealing temperature on the photoluminescence from silicon nitride multilayer structures”, *J. Cryst. Growth*, **310**(15), 3680-3684.
- Sergo, V., Pezzotti, G., Katagiri, G., Muraki, N. and Nishida, T. (1996), “Stress dependence of the raman spectrum of  $\beta$ -silicon nitride”, *J. Am. Ceram. Soc.*, **79**(3), 781-784.
- Sung, G.Y., Park, N.M., Shin, J.H., Kim, K.H., Kim, T.Y., Cho, K.S. and Huh, C. (2006), “Physics and device structures of highly efficient silicon quantum dots based silicon nitride light-emitting diodes”, *IEEE J. Sel. Top. Quant. Elect.*, **12**(6), 1545-1555.
- Temple, P.A. and Hathaway, C.E. (1973), “Multiphonon raman spectrum of silicon”, *Phys. Rev. B*, **7**(8), 3685-3696.
- Tomar, V.K., Patil, L.S. and Guatam, D.K. (2008), “Deposition and characterization of silicon nitride films using HMDS for photonics applications”, *J. Optoelectron. Adv. Mater.*, **10**(10), 2657-2662.
- Torchynska, T.V. (2010), “Nanocrystals and quantum dots. Some physical aspects”, In: *Nanocrystals and Quantum Dots of Group IV Semiconductors*, (T.V. Torchynska, Yu Vorobiev Eds.), American Scientific Publisher, Stevenson Ranch, CA, USA.
- Torchynska, T.V., Korsunskaya, N.E., Dzhumaev, B.R. and Khomenkova, L.Yu. (2000a), “Three approaches to surface substance role investigation in porous silicon photoluminescence and its excitation”, *J. Phys. Chem. Solid*, **61**(6), 937-941.
- Torchynska, T.V., Palacios Gomez, J., Polupan, G.P., Garcia Borquez, A., Korsunskaya, N.E. and Khomenkova, L.Yu. (2000b), “Complex nature of the red photoluminescence band and peculiarities of its excitation in porous silicon”, *Appl. Surf. Sci.*, **167**(3), 197-204.
- Torchynska, T.V., Casas Espinola, J.L., Vergara Hernandez, E., Khomenkova, L., Delachat, F. and Slaoui, A. (2015a), “Effect of the stoichiometry of Si-rich silicon nitride thin films on their photoluminescence and structural properties”, *Thin Solid Films*, **581**, 65-69.
- Torchynska, T.V., Casas Espinola, J.L., Khomenkova, L., Vergara Hernandez, E., Andraca Adame, J.A. and Slaoui, A. (2015b), “Structural and light emitting properties of silicon-rich silicon nitride films grown by plasma enhanced-chemical vapor deposition”, *Mater. Sci. Semicond. Proces.*, **37**, 46-50.
- Tsu, D.V., Lucovsky, G. and Mantini, M.J. (1986), “Local atomic structure in thin films of silicon nitride and silicon diimide produced by remote plasma-enhanced chemical-vapor deposition”, *Phys. Rev. B*, **33**(10), 7069-7074.
- Walters, R.J., Bourianoff, G.I. and Atwater, H.A. (2005), “Field-effect electroluminescence in silicon nanocrystals”, *Nat. Mater.*, **4**(2), 143-146.
- Wang, Y.Q., Wang, Y.G., Cao, L. and Cao, Z.X. (2003), “High-efficiency visible photoluminescence from amorphous silicon nanoparticles embedded in silicon nitride”, *Appl. Phys. Lett.*, **83**(17), 3474-3476.
- Wang, M., Li, D., Yuan, Zh., Yang, D. and Que, D. (2007), “Photoluminescence of Si-rich silicon nitride:

- Defect-related states and silicon nanoclusters”, *Appl. Phys. Lett.*, **90**(13), 131903.
- Warren, W.I., Lenahan, P.M. and Curry, S.E. (1990), “First observation of paramagnetic nitrogen dangling-bond centers in silicon nitride”, *Phys. Rev. Lett.*, **65**(2), 207-210.
- Wenge, D., Wenhao, Q.I., Wanbing, L.U., Zicai, Zh., Wei, Y.U. and Guangsheng, F.U. (2008), “Influence of annealing environment on the Hydrogen related bonding structure in silicon nitride thin films containing silicon nanoparticles”, *Proceedings of SPIE*, Volume 7135, 71353X-1.
- Wolkin, M.V., Jorne, J., Fauchet, P.M., Allan, G. and Delerue, C. (1999), “Electronic states and luminescence in porous silicon quantum dots: the role of oxygen”, *Phys. Rev. Lett.*, **82**(1), 197-200.
- Zeng, X., Liao, W., Wen, G., Wen, X. and Zheng, W. (2014), “Structural evolution and photoluminescence of annealed Si-rich nitride with Si quantum dots prepared by plasma enhanced chemical vapor deposition”, *J. Appl. Phys.*, **115**(15), 154314.